Magnetic Reversal of Electric Polarization with Fixed Chirality of Magnetic Structure in a Chiral-Lattice Helimagnet MnSb_{2}O_{6}

M. Kinoshita, S. Seki, T. J. Sato, Y. Nambu, T. Hong, M. Matsuda, H. B. Cao, S. Ishiwata, and Y. Tokura

Phys. Rev. Lett. **117**, 047201 — Published 22 July 2016

DOI: 10.1103/PhysRevLett.117.047201

Magnetic reversal of electric polarization with fixed chirality of magnetic structure in a chiral-lattice helimagnet $MnSb_2O_6$

M. Kinoshita[1], S. Seki[2,3],* T. J. Sato[4], Y. Nambu[4],† T. Hong[5],
M. Matsuda[5], H. B. Cao[5], S. Ishiwata[1,3], and Y. Tokura[1,2]

[1] *Department of Applied Physics and Quantum Phase Electronics Center (QPEC), University of Tokyo, Tokyo 113-8656, Japan*

[2] *RIKEN Center for Emergent Matter Science (CEMS), Wako 351-0198, Japan*

[3] *PRESTO, Japan Science and Technology Agency (JST), Tokyo 102-8666, Japan*

[4] *Institute of Multidisciplinary Research for Advanced Materials, Tohoku University, Sendai 980-8577, Japan and*

[5] *Quantum Condensed Matter Division, Oak Ridge National Laboratory, Oak Ridge, TN 37831,USA*

(Dated:)

Abstract

The correlation between magnetic and dielectric properties has been investigated for the single crystal of chiral triangular-lattice helimagnet $MnSb_2O_6$. We found that the spin-spiral plane in the ground state has a considerable tilting from the (110) plane, and that the sign of spin-spiral tilting angle is coupled to the clockwise/counter-clockwise manner of spin rotation and accordingly to the sign of magnetically-induced electric polarization. This leads to unique magnetoelectric responses such as magnetic-field-induced selection of a single ferroelectric domain as well as reversal of electric polarization just by a slight tilting of magnetic field direction, where the chiral nature of the crystal structure plays a crucial role through the coupling of the chirality between the crystal and magnetic structures. Our results demonstrate that the crystallographic chirality can be an abundant source of novel magnetoelectric functions with coupled internal degrees of freedom.

PACS numbers: 75.85.+t

The magnetoelectric (ME) effect, i.e. magnetic control of dielectric properties or electric control of magnetism, has attracted revived interests[1–3]. One of late breakthroughs is the discovery of magnetically-induced ferroelectricity originating from the symmetry breaking by the helical magnetic structure, where the strong coupling between the magnetic structure and electric polarization P leads to unprecedentedly large and versatile ME effects[4–9]. The above phenomenon has first experimentally been reported for a group of frustrated magnets with centrosymmetric crystallographic lattice[4, 10–12], where the clockwise/counter-clockwise manner of helical spin rotation (i.e. spin helicity) is found to be coupled with the sign of electric polarization[7, 13, 14].

Recently, the emergence of nontrivial magnetic structure has also been reported for a series of magnetic materials with chiral crystallographic lattice, which holds no inversion center nor mirror plane and has the distinction between the right-handed and left-handed crystal. In the chiral-lattice ferromagnets, Dzyaloshinskii-Moriya (DM) interaction favoring the mutually canted spin arrangement leads to the formation of chiral magnetic structures such as magnetic skyrmion[15–20] or chiral soliton lattice[21, 22], both of which are now the subject of extensive research as the potential information carriers. Likewise, the chiral-lattice antiferromagnets also host unique magnetic structure characterized by chirality[23, 24]. One typical example is the triangular-lattice antiferromagnet $Ba_3NbFe_3Si_2O_{14}$, which stabilizes the in-plane 120° spin order with helical spin modulation along the out-of-plane direction[23]. In this compound, the chirality of magnetic structure is always single-handed and coupled to the underlying crystallographic chirality, because of the asymmetric distribution of exchange interactions. Since the chirality of magnetic structure is closely related with the spin helicity and the associated sign of electric polarization, such chiral-lattice materials are anticipated to host distinctive magnetoelectric responses as compared with the centrosymmetric materials.

The present target material $MnSb_2O_6$ is another example of chiral-lattice antiferromagnets of insulating nature, and its crystal structure belongs to chiral trigonal space group $P321$ (Fig. 1 (a))[25, 26]. The magnetism is dominated by the triangular lattice of Mn^{2+} ions ($S = 5/2$) stacked along the [001] axis, and helical spin order with magnetic modulation vector $\vec{q} \sim (0, 0, 0.182)$ is stabilized below 12 K due to the frustration among multiple paths of exchange interaction (Fig. 1 (c))[27]. Here, we define $\vec{S}_i$ and $\vec{S}_j$ as the adjacent Mn spins along the c-axis, and the spin-spiral plane is normal to the vector $(\vec{S}_i \times \vec{S}_j)$. The previous neutron diffraction study[27] proposed that the magnetic moments rotate in a common plane

including the [001] axis. Three spin-cycloids in the unit cell have the same manner of spin rotation along the out-of-plane direction, which is represented by the vector[27]

$$\vec{P}_m = \vec{q} \times (\vec{S}_i \times \vec{S}_j). \tag{1}$$

Mn spins also form the 120° spin order on the triangular lattice plane due to magnetic frustration, where the spin rotation on triangular Mn atoms is either $0 \rightarrow (2/3)\pi \rightarrow (4/3)\pi$ or $0 \rightarrow (4/3)\pi \rightarrow (2/3)\pi$. The spin-rotation sense along the in-plane direction can be described by the vector[27]

$$\vec{A} = \vec{q} \times (\vec{S}_1 \times \vec{S}_2 + \vec{S}_2 \times \vec{S}_3 + \vec{S}_3 \times \vec{S}_1), \tag{2}$$

with $\vec{S}_1$, $\vec{S}_2$, and $\vec{S}_3$ being the spins on the triangle. By definition, $\vec{A}$ and $\vec{P}_m$ are always parallel or antiparallel, and the sign of the dot product $\vec{A} \cdot \vec{P}_m$ reflects the overall chirality of magnetic structure. So far, the emergence of magnetically-induced electric polarization, as well as the single-handed nature of chiral magnetic structure, have not been established experimentally for this compound.

In this Letter, we have investigated the magnetoelectric properties for the single crystal of chiral triangular-lattice helimagnet $MnSb_2O_6$. We found that the spin-spiral plane in the ground state has a considerable tilting from the previously proposed (110) plane by angle θ_t, whose sign turns out to be coupled to the spin helicity along both in-plane and out-of-plane directions (i.e. $\vec{A}$ and $\vec{P}_m$) as well as the sign of magnetically-induced electric polarization. The corresponding magnetic-field (H) direction dependent reversal of electric polarization has been successfully detected, while the detailed analysis of neutron diffraction data suggests that the overall chirality of magnetic structure (i.e. $\vec{A} \cdot \vec{P}_m$) is always fixed in this chiral-lattice compound. Such an unusual manner of H-induced switch of electric polarization and spin helicity highlights chiral-lattice magnets as the source of unique magnetoelectric functions with coupled internal degrees of freedom.

The single crystals of $MnSb_2O_6$ up to 2.6 mm × 2.6 mm ×1.2 mm were grown by a flux method[26]. They were cut into a rectangular shape and silver paste was painted on a pair of the $(1\bar{1}0)$ surfaces as electrodes. To deduce the electric polarization P, we measured the polarization current I with a constant rate of H-rotation (1.2 °/sec) and integrated it with time t. Magnetization M was measured with Magnetic Properties Measurement System (MPMS, Quantum Design Inc.). The setup for neutron diffraction experiments is provided in Supplemental Material.

Figure 1 (b) shows the temperature (T) dependence of magnetic susceptibility $\chi(= M/H)$ for H along the [110] axis and the [001] axis. In both cases, χ shows a clear anomaly at the Néel temperature $T_{\rm N} \sim 12$ K, which signals the onset of magnetic order. To check the validity of the previously proposed ac-cycloidal magnetic structure[27], H-direction dependence of χ is measured at 4 K under the various magnitudes of H rotating within the $(1\bar{1}0)$ plane (Fig. 2 (a)). Here, we define θ_H as the angle between the H-direction and the [110] axis. While χ-profile shows almost sinusoidal behavior against θ_H with its maximal (minimal) peaks at $\theta_H = (180n)^\circ$ ($\theta_H = (180n + 90)^\circ$) in the low-$H$ region (n: integer), these peak structures show clear splitting in the higher H region above 0.6 T. The spin-spiral plane generally prefers to keep its direction normal to H to maximize the energy gain by the Zeeman term, while it is prevented by magnetic anisotropy in particular for the low-H region. As H increases, the spin-spiral plane shows larger tilting and finally the H-induced smooth rotation satisfying the relationship $(\vec{S}_i \times \vec{S}_j) \parallel \vec{H}$ becomes possible. In the latter situation, χ is expected to take the maximum (minimum) value when the applied H is normal (parallel) to the original spin-spiral plane in the ground state. Thus, the observed splitting of the χ peak structures suggests that the spin-spiral plane in the ground state of $MnSb_2O_6$ is not exactly within the plane including the [001] axis, but rather slightly tilted from it (Figs. 1 (c) and (e)). Based on the obtained peak interval, the tilting angle of spin-spiral plane from the (110) plane is estimated to be around $\theta_t \sim 13^\circ$. Note that the contribution of the magnetic anisotropy becomes negligible in the limit of large H, which explains the observed suppression of the χ-anomalies above 1.5 T.

The model of tilted cycloidal magnetic structure (Figs. 1 (c) and (e)) is also consistent with our result of magnetic structure analysis based on neutron diffraction experiments on single crystal of $MnSb_2O_6$. While the previous neutron diffraction study[27] assumed that $(\vec{S}_i \times \vec{S}_j)$ is exactly normal to the c-axis, we have considered the possibility that $(\vec{S}_i \times \vec{S}_j)$ can be tilted from the [110] axis toward the [001] axis by angle θ_t. The best fit is obtained for $\theta_t \sim 18^\circ$ (Fig. 2(b)), which roughly agrees with $\theta_t \sim 13^\circ$ deduced from the magnetization measurements. One possible origin of such a spin-spiral tilting is the magnetic anisotropy term of the fourth or higher order, which has been proposed to cause the tilting of spin-spiral plane from the three-fold rotation axis in case of chiral cubic lattice systems[15, 16].

As discussed in Ref. [27], the single-crystal unpolarized neutron diffraction intensities depend on the dot product $\vec{A} \cdot \vec{P}_m$, but are insensitive to the individual orientation of $\vec{A}$ and

$\vec{P}_m$. Here, we label the domains with positive and negative sign of $\vec{A}\cdot\vec{P}_m$ as MD1 and MD2. While the previous neutron diffraction study[27] reported the coexistence of MD1 and MD2 domains with the ratio of 8:2 (possibly due to the mixture of opposite chiral crystallographic domains in the measured sample), the present analysis revealed that MD1 is dominant and that the population of MD2 is less than 1% in our $MnSb_2O_6$ single crystal. Since the sign of $\vec{A}\cdot\vec{P}_m$ reflects the overall chirality of magnetic structure, our results firmly establish the single-handed nature of chiral magnetic structure in the present compound. Recent calculations based on the density functional theory[27] have proposed that the diagonal paths of exchange interaction hold the chiral asymmetry in $MnSb_2O_6$, which may explain the observed coupling between the magnetic and crystallographic chirality.

As recently reported for several helimagnets[4, 5, 10–12], the cycloidal magnetic order often induces electric polarization $\vec{P} = \alpha\vec{P}_m$ through the inverse Dzyaloshinskii-Moriya mechanism[7–9] with α being a coupling constant inherent to the underlying crystal lattice and electronic structures. Given the cycloidal magnetic structure with $(\vec{S}_i \times \vec{S}_j)$ tilted from the [110] axis toward the [001] axis, P is expected to appear along the $[1\bar{1}0]$ direction according to Eq. (1) (Figs. 1(c) and (e)). Note that the trigonal $MnSb_2O_6$ should host a plural number of equivalent helimagnetic domains, which are mutually converted by symmetry operations that are possessed by the original crystal structure[28]. For example, the application of two-fold rotation around the [110] axis reverses the sign of both tilting angle θ_t and the associated P (Figs. 1(d) and (f)). Correspondingly, both $\vec{P}_m$ and $\vec{A}$ are also reversed, while the overall chirality of magnetic structure (i.e. $\vec{A}\cdot\vec{P}_m$) remains unchanged. We label these two domains with opposite sign of tilting angle θ_t as (+) and (−) domains (Figs. 1(e) and (f)). Likewise, the three-fold rotation around the [001] axis triples the number of domains. As a result, we can deduce six equivalent helimagnetic domains characterized by different orientations of spin-spiral plane, which directly correspond to six ferroelectric domains with unique $P \parallel \langle 1\bar{1}0\rangle$ directions as summarized in Fig. 1 (g). While the total P will cancel out under the coexistence of these domains for $H = 0$, the application of H should lift their degeneracy and thus can select a single ferroelectric domain with nonzero P (Figs. 1 (h) and (i)). Note that the tilting of spin-spiral plane is essential for H-induced control of domains or associated P, since H cannot distinguish the (+) and (−) domains (i.e. $\pm P$ domains) without spin-spiral tilting.

Such H-induced domain rearrangement can be detected in the magnetization profiles.

Figures 3 (a)-(d) indicate the H-dependence of M and the corresponding H-derivative of M (dM/dH) at various temperatures for $H \parallel [001]$ and $H \parallel [110]$. For $H \parallel [001]$, M shows an almost H-linear behavior, but a step-like anomaly at around 1 T. This can be assigned to a kind of spin-flop transition, where the applied H reorients the spin-spiral plane into the ab-plane. On the other hand, the small anomaly in M-profile is observed for $H \parallel [110]$ at around 0.2 T, which can be ascribed to the selection of a single pair of the (+) and (−) domains with the spin-spiral plane nearly perpendicular to H. On the basis of the obtained anomalies in the $M-T$ and $M-H$ profiles, we have summarized the $H-T$ magnetic phase diagram for both $H \parallel [001]$ and $H \parallel [110]$, as shown in Figs. 3 (e) and (f), respectively.

To establish the magnetoelectric nature of $MnSb_2O_6$, we have further measured the electric polarization P (by taking the time integration of pyroelectric current I) along the $[1\bar{1}0]$ axis under the H rotating within the $(1\bar{1}0)$ plane (Figs. 4 (a) and (b)). For a while, we discuss the behavior at $\mu_0 H = 1.5$ T, where the spin-spiral plane is expected to be always normal to H-direction (i.e. $(\vec{S}_i \times \vec{S}_j) \parallel \vec{H}$) as shown by the aforementioned magnetization measurements. The θ_H-dependent change of I and P with the period of 180° has successfully been detected, and the clear peak structure in the I-profile as well as the step-like anomaly in the P-profile appear at $\theta_H = (180n)°$. In this process, a pair of (+) and (−) domains characterized by opposite sign of P and θ_t (Figs. 1 (e) and (f)) are relevant. To minimize the H-induced additional tilting of spin-spiral plane from the original magnetic structure, the (+) domain is selected for $(180n)° < \theta_H < (180n + 90)°$ and the (−) domain is for $(180n + 90)° < \theta_H < (180n + 180)°$ as schematically shown in Fig. 4 (d). Considering the corresponding H-induced switching between the (+) and (−) domains as well as the rotation of spin-spiral plane, we can expect $P = -P_0 \cos\theta_H$ for $(360n)° < \theta_H < (360n + 180)°$ and $P = +P_0 \cos\theta_H$ for $(360n + 180)° < \theta_H < (360n + 360)°$ based on Eq. (1) with P_0 being a coupling constant. Such a predicted P-behavior is plotted in Fig. 4 (b) with a dashed line, which explains the experimentally observed feature for $\mu_0 H = 1.5$ T. When H is decreased, the additional I-peak as well as P-step can be detected at $\theta_H = (180n + 90)°$. For this θ_H-value (i.e. $H \parallel c$) with sufficiently large magnitude of H, the spin-spiral plane prefers to lie within the (001) plane and Eq. (1) gives $P = 0$ for both (+) and (−) domains, leading to the absence of P anomaly associated with the (+)/(−) domain switching (Fig. 4 (f)). With the smaller magnitude of H, however, the spin-spiral plane cannot orient exactly normal to $H \parallel c$. Thus, the finite magnitude of P remains around this θ_H value and it causes the sharp

anomaly upon the domain switching (Fig. 4 (e)). With $\mu_0 H < 0.3$ T, the domain selection itself becomes impossible, therefore the signals in the I- and P-profiles vanish (Fig. 4 (c)) [29].

In summary, we have experimentally proved the multiferroic nature of the chiral-lattice antiferromagnet $MnSb_2O_6$, and found the appearance of tilted cycloidal magnetic structure with fixed chirality. Unlike the conventional case of spin-driven ferroelectrics with originally centrosymmetric crystal lattice[4, 5, 10–12], $MnSb_2O_6$ with chiral crystal lattice shows unique magnetoelectric responses: (1) A single ferroelectric domain can be realized with no external electric field but only magnetic field as low as 0.3 T. (2) The sign of electric polarization (and associated spin helicity) can be reversed just by a slight tilting of magnetic field direction from the [110]-axis. For these unusual magnetoelectric behaviors, the chiral nature of the crystal structure plays a crucial role through the coupling of the chirality between the crystal and magnetic structures. Our present results demonstrate that the crystallographic chirality can be an abundant source of novel magnetoelectric functions with coupled internal degrees of freedom.

The authors thank H. Sakai, T. Kurumaji, N. Nagaosa and T. Arima for enlightening discussions and experimental helps. This work was partly supported by the Mitsubishi Foundation, Grants-In-Aid for Scientific Research (Grant No. 26610109, 15H05458, 24224009, 16K13842) from the MEXT of Japan, and FIRST Program by the Japan Society for the Promotion of Science (JSPS). The work at the HFIR, Oak Ridge National Laboratory, was sponsored by the Division of Scientific User Facilities, Office of Basic Energy Science, US Department of Energy (DOE), and was supported by the US-Japan Cooperative Program on Neutron Scattering.

* Corresponding author: shinichiro.seki@riken.jp

† Present address: Institute for Materials Research, Tohoku University, Sendai 980-8577, Japan

[1] M. Fiebig, J. Phys. D: Appl. Phys. **38**, R123 (2005).

[2] S. W. Cheong, M. Mostovoy, Nature Mater. **6**, 13 (2007).

[3] Y. Tokura, S. Seki, N. Nagaosa, Rep. Prog. Phys. **77**, 076501 (2014).

[4] T. Kimura *et al.*, Nature **426**, 55 (2003).

[5] M. Kenzelmann *et al.*, Phys. Rev. Lett. **95**, 087206 (2005).

[6] N. Hur *et al.*, Nature (London) **429,** 392 (2004)

[7] H. Katsura, N. Nagaosa, A. V. Balatsky, Phys. Rev. Lett. **95**, 057205 (2005).

[8] M. Mostovoy, Phys. Rev. Lett. **96**, 067601 (2006).

[9] I. A. Sergienko and E. Dagotto, Phys. Rev. B **73**, 094434 (2006).

[10] G. Lawes *et al.*, Phys. Rev. Lett. **95**, 087205 (2005).

[11] K. Taniguchi *et al.*, Phys. Rev. Lett. **97,** 097203 (2006).

[12] T. Kimura *et al.*, Phys. Rev. Lett. **94,** 137201(2005).

[13] Y. Yamasaki *et al.*, Phys. Rev. Lett. **98**, 147204 (2007).

[14] S. Seki *et al.*, Phys. Rev. Lett. **100**, 127201 (2008).

[15] S. Mühlbauer *et al.*, Science **323**, 915 (2009).

[16] W. Münzer *et al.*, Phys. Rev. B **81**, 041203(R) (2010).

[17] X. Z. Yu *et al.*, Nature Mater. **10**, 106 (2011).

[18] S. Seki *et al.*, Science **336**, 198 (2012).

[19] S. Seki, S. Ishiwata, Y. Tokura, Phys. Rev. B **86**, 060403(R) (2012).

[20] U. K. Rößler, A. N. Bogdanov, C. Pfleiderer, Nature **442**, 797 (2006).

[21] Y. Togawa *et al.*, Phys. Rev. Lett. **108**, 107202 (2012).

[22] J. Kishine, I. V. Proskurin, A. S. Ovchinnikov, Phys. Rev. Lett. **107**, 017205 (2011).

[23] K. Marty *et al.*, Phys. Rev. Lett. **101**, 247201 (2008).

[24] M. Janoschek *et al.*, Phys. Rev. B **81**, 094429 (2010).

[25] J. N. Reimers, J. E. Greedan, M. A. Subramanian, J. Solid. State. Chem. **79**, 263 (1989).

[26] A. M. Nakua, J. E. Greedan, J. Cryst. Growth **154**, 334 (1995).

[27] R. D. Johnson *et al.*, Phys. Rev. Lett. **111**, 017202 (2013).

[28] H. Schmid *et al.*, J. Phys.: Condens. Matter **20**, 434201 (2008).

[29] For $\mu_0 H < 0.3$ T, the coexistence of the (+) and (−) domains also masks the overall anisotropy associated with the spin-spiral tilting in the $\chi - \theta_H$ profile (Fig. 2(a)).

Figures

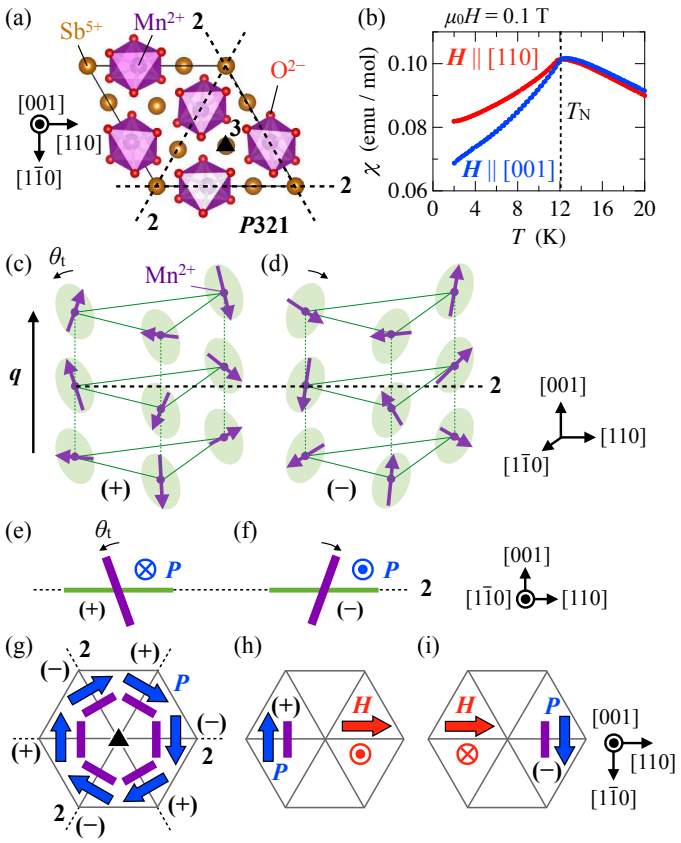

FIG. 1: (color online). (a) Crystal structure of $MnSb_2O_6$ with chiral trigonal space group $P321$. The compatible symmetry elements (two-fold rotation axes (2) along the $\langle 110 \rangle$ directions and three-fold rotation axis (closed triangle) along the [001] direction) are also indicated. (b) Temperature dependence of magnetic susceptibility for $H \parallel [110]$ and $H \parallel [001]$. (c) Schematic illustration of helical magnetic structure in the ground state of $MnSb_2O_6$, with its spin-spiral plane tilted from the (110) plane by angle θ_t. The application of two-fold rotation around the [110] axis gives equivalent magnetic structure as shown in (d). These two domains (i.e. the (+) and (−) domains) are characterized by the opposite sign of spin-spiral tilting angle θ_t and magnetically-induced electric polarization $P \parallel [1\bar{1}0]$. The views from the $[1\bar{1}0]$ direction are also shown in (e) and (f). (g) Six equivalent helimagnetic domains characterized by different orientation of spin-spiral plane (purple bold bars). The sign of θ_t for each domain is expressed by (+) and (−). The corresponding orientation of magnetically-induced electric polarization $P \parallel \langle 1\bar{1}0 \rangle$ are also indicated with blue arrows. (h) and (i) Examples of the favored domain configuration under the specific external H having both in-plane and out-of-plane components (red arrows and symbols).

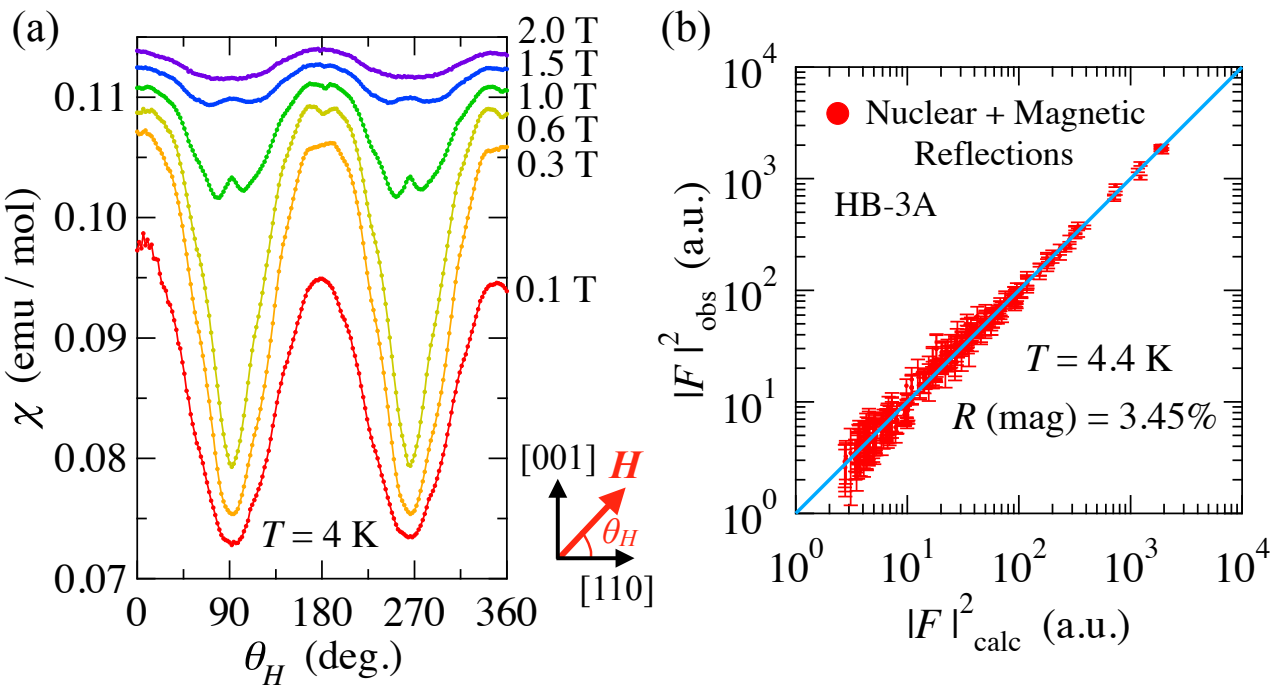

FIG. 2: (color online). (a) H-direction dependence of magnetic susceptibility measured at 4 K with various magnitudes of H. Here, H is rotated within the $(1\bar{1}0)$ plane and θ_H is defined as the angle between the [110] axis and H-direction. Before each measurement, the sample is cooled down from 20 K to 4 K with $\mu_0 H = 2$ T at $\theta_H = 0°$, and then the magnitude of H is tuned at the target value to align the three-fold helimagnetic domains. The data are arbitrarily shifted along the vertical axes. (b) Calculated versus observed intensities for both the nuclear and magnetic reflections obtained by single-crystal neutron diffraction experiments for the magnetic structure shown in Fig. 1 (c) with $\theta_t \sim 18°$. For the detail of neutron diffraction experiments, see Supplemental Material.

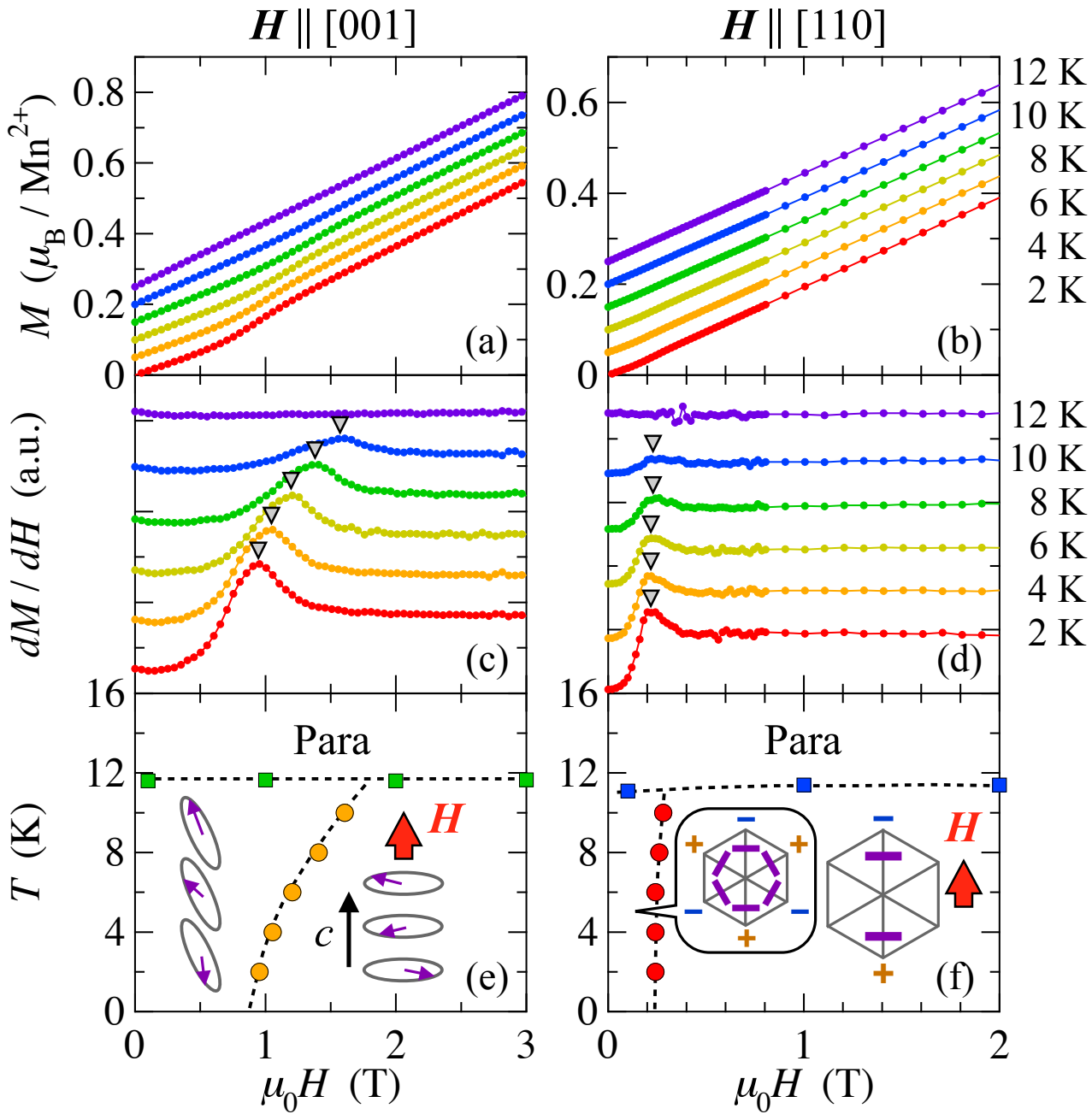

FIG. 3: (color online). Magnetic field dependence of magnetization M for (a) $H \parallel [001]$ and (b) $H \parallel [110]$, measured at various temperatures after the zero field cooling. The corresponding H-derivative of M are plotted in (c) and (d), whose anomalies represent spin-flop transitions and domain selections, respectively. The data are arbitrarily shifted along the vertical axes. Based on the anomalies found in the $M-T$ (squares) and $M-H$ (circles) profiles, $H-T$ magnetic phase diagrams are summarized in (e) and (f).

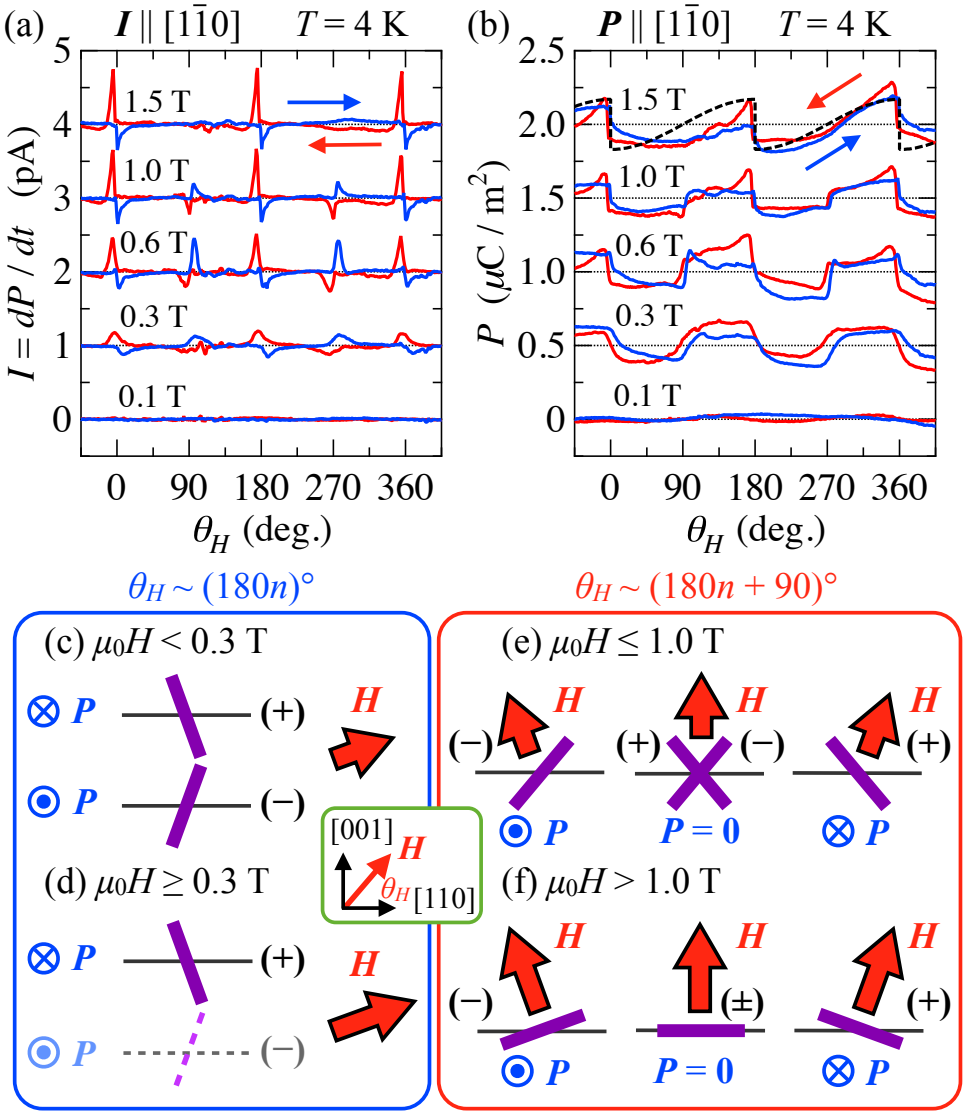

FIG. 4: (color online). (a) H-direction dependence of polarization current I and (b) corresponding electric polarization P, measured along the [1$\bar{1}$0] direction at 4 K with various magnitudes of H. The definition of θ_H is common with the case for Fig. 2 (a), and all the measurements were performed after once applying in-plane $\mu_0 H \sim 2$ T at 4 K. The arrows indicate the direction of H-rotation, and the data are arbitrarily shifted along the vertical axes. Here, theoretically expected behaviors based on Eq. (1) under the assumption of $(\vec{S}_i \times \vec{S}_j) \parallel \vec{H}$ are also plotted with a dashed line. (c)-(f) Schematic illustration of the H-induced (+)/(−) domain switching. (c) and (d) are for the case of $\theta_H \sim (180n)°$, and (e) and (f) for the case of $\theta_H \sim (180n + 90)°$. Depending on the magnitude of H, different behaviors of P-generation can be observed for the respective cases.